Phys Chem Minerals (2001) 28: 130–141

ORIGINAL PAPER

C. I. Sainz-Diaz · A. Hernández-Laguna · M. T. Dove

Modeling of dioctahedral 2:1 phyllosilicates by means of transferable empirical potentials

Received: 8 March 2000 / Accepted: 19 September 2000

Abstract Dioctahedral 2:1 phyllosilicates with different interlayer charge have been studied theoretically by using transferable empirical interatomic potentials. The crystal structures of pyrophyllite, muscovite, margarite, beidellite, montmorillonite, and different smectites and illites have been simulated. The interatomic potentials were able to reproduce the experimental structure of phyllosilicates with high, medium and low interlayer charge. The calculated structures are in agreement with experiment for the main structural features of the crystal lattice. The effect of the cation substitution in the octahedral and tetrahedral sheets on the structural features has been also studied. Good linear relationships have been found, and the calculated effects are consistent with experimental results. Some unknown structural features of the crystal structures of clays are predicted in this work.

Key words Dioctahedral 2:1 phyllosilicates · Pyrophyllite · Mica · Smectite/illite · Theoretical study · Crystal structure · Cation substitution effect

Introduction

Smectites and other related 2:1 phyllosilicate clay minerals share the common structural feature that single sheets of octahedrally coordinated cations are sandwiched between two layers of tetrahedra. The great diversity of these silicates occurs because of their capacity for isomorphous substitution of various cation in octahedral and tetrahedral sheets, providing different properties in the interlayer space. These substitutions include Al^{3+} by Mg^{2+} in the octahedral sheet, together with Si^{4+} by Al^{3+} in the tetrahedral sheet, and result in a net negative charge. This charge is compensated by the presence of additional cations in the interlayer space. In this space, the cations can be exchanged easily, and different molecules of water or organics can be swelled. The cation substitutions (in octahedral and tetrahedral sheets) create disordering phenomena in the crystal lattice structure of these minerals. The cation distribution in the tetrahedral (Herrero and Sanz 1991) and octahedral (Cuadros et al. 1999) sheets of these minerals has been studied previously. One additional type of structural disorder is the distribution of the layers. The geometrical similarity of these layer silicate structures facilitates the formation of structures containing different kinds of layers and different ordered and disordered sequences of layers. All these types of structural disorder and the small size of the crystals in clays make it difficult to obtain good experimental structural data for these minerals by X-ray, neutron, or electron diffraction techniques, especially in smectites and illites. The valuable catalytic and adsorptive properties of clays urge us towards having an interest in establishing a firm theoretical understanding of their structure and behaviour. This study can also be useful to understand some mineral transformations and some industrial applications of clays, like catalysis, and nuclear waste and pollutant disposal barrier component.

Computer simulations can contribute significantly in achieving an understanding of structure-property relationships in these systems. These theoretical studies require a model of the forces acting between the atoms in the mineral. Despite the increasing applicability of first-principles quantum-mechanical methods based on periodic density functional and Hartree-Fock methods to the solid state, the computational effort of these methods limits their application to large systems with low symmetry such as clays (Sauer et al. 1994). Atomistic calculations with empirical potentials based on the Born

C. I. Sainz-Diaz (✉) · A. Hernández-Laguna
Estacion Experimental del Zaidin (CSIC),
C/ Profesor Albareda, 1. 18008-Granada, Spain
Fax: +34 958 129600
e-mail: sainz@eez.csic.es

M. T. Dove
Department of Earth Sciences,
University of Cambridge, Downing Street,
Cambridge CB2 3EQ, UK

model of the ionic lattice, which employ interatomic potentials to represent the short-range interactions between ions, are fast and provide sufficient accuracy for reproducing properties of many ionic solids. These potentials are Coulomb interactions between the ionic charges and a short-range function, which describes the non-Coulombic interactions between ions, that is the Pauli repulsion at short range and the dispersion forces at longer ranges. These empirical potentials can be obtained by different methods, e.g. fitting the form of the chosen potential model to experimental data (Abbot et al. 1989a, b; Collins and Catlow 1992), ab initio quantum-mechanical calculations (Lasaga and Gibbs 1987), and modified electron gas calculations (Post and Burnham 1986). These potentials obtained for one solid should be transferable to other similar solids if these computational modeling techniques are to be used as predictive methods. This approach has been applied with good results in a number of silicates: quartz zeolites (Schröder et al. 1992), forsterite (Price and Parker 1988), and several framework silicates (Dove 1989; Winkler et al. 1991). Computational simulation methods have been applied to studies of layered phyllosilicates with high interlayer charge, like muscovite (Collins and Catlow 1992). However, only a few studies have been applied to phyllosilicates with low interlayer charge (Teppen et al. 1997), and some unsatisfactory results have been reported (Collins 1990), since it is difficult to reproduce the hydrogen bonding and the weak interactions of the interlayer space of these minerals. One of the aims of this work is to find a suitable model for reproducing the experimental structure of phyllosilicates with low interlayer charge and thus, to assess the transferability of certain previously published interatomic potentials for modeling the structures of these complex minerals.

We report on a wide range of materials. In most cases we are able to obtain reasonably good agreement with experimental data, and can account for trends in structural details with chemical composition. We are able to extend the range of calculations beyond the systems for which there are experimental data in order to be able to predict the crystal structures of materials for which experimental structural data are difficult to obtain. We will find that problems with the models arise only when there are no interlayer cations, where the interlayer spacing depends only on weak dispersive interactions.

The objective of our work is to establish the ability of the models to simulate a wide range of chemical compositions in layer silicates as a prelude to further studies. We have an active programme of work on the energetics and mechanisms of cation ordering that requires a well-tested model. For example, we have used the models discussed here to perform calculations on Al/Si ordering in the tetrahedral layers of muscovite, and on coupled Al/Si tetrahedral and Mg/Al octahedral ordering in phengite, obtaining results that are in excellent agreement with several sets of experimental data (EV Palin et al. submitted 2000).

Methods

The basic interatomic potential model has been described previously elsewhere (Winkler et al. 1991; Collins and Catlow 1992). Electrostatic Coulomb interactions are evaluated by the Ewald method using formal charges in the ions. In modeling the oxygen ions, electronic polarizability effects are taken into account by using the core-shell model, where a massless shell is linked to the core by ideal harmonic interactions ($U_s = 1/2K_s r^2, K_s$ is the harmonic spring constant and r is the core-shell separation). The cation core–O_{shell} and O_{shell}–O_{shell} short-range interactions are described by Buckingham potentials:

$$U_{sr} = A\exp(-r/\rho) - Cr^{-6} \quad , \tag{1}$$

where the exponential term describes the repulsive energy and the r^{-6} term the longer-range attraction. The intramolecular OH interaction is described by a Morse potential:

$$U_{sr} = \varepsilon\{1 - \exp[-\alpha(r-\mu)]\}^2 \quad , \tag{2}$$

where r and μ are the observed and equilibrium interatomic distances, respectively. Coulomb forces are not included between atoms coupled by a Morse potential, as it is assumed that this potential describes all components of the interactions between both atoms.

Covalent effects are simulated using three-body bond-bending interactions:

$$U_{tbsr} = 1/2K_{tbsr}(\theta - \theta_0)^2 \quad , \tag{3}$$

where K_{tbsr} is the harmonic three-body force constant, and θ and θ_o are the observed and ideal bond angles, respectively). All these potentials use full integral charges on all atoms except for the OH species, whose component atoms have partial charges chosen so as to reproduce the dipole moment of the OH group. The values of the parameters for the potentials used in this work are described in Table 1. An empirical Al^{3+}–O^{2-} potential (Catlow et al. 1982) has been used for all coordinations (Jackson and Catlow 1988). Although the OH groups are joined to cations of the octahedral sheet, they are also close to the cations of the tetrahedral sheet. Then, we include an empirical Si^{4+}_{core}–$O^{1.426-}_{core}$ potential for the Si/OH interactions (Collins and Catlow 1992), and an Al^{3+}_{core}–$O^{1.426-}_{core}$ potential for the tetrahedral Al/OH interactions (Schröder et al. 1992). Since the isomorphous substitution of Mg and Fe occurs in the octahedral sheet, the Mg–O and Fe–O potentials were also included for both types of oxygens (O^{2-} and OH). The long-range H bonds (OH. . .O) are described by an H–O Buckingham potential (Winkler et al. 1991). All these parameters have been used to model accurately structures and crystal properties of the main rock-forming silicate minerals (see references in Table 1). In the case of the illite/smectite studies, a careful selection of parameters was necessary, particularly to describe properly the interlayer cation-oxygen potentials and the interlayer space, as is discussed below. All lattice-energy calculations have been performed by means of the GULP code (Gale 1997). The Newton-Raphson minimization method was used for the lattice relaxation.

Previous experimental studies on micas found a random distribution of cations in the tetrahedral sheet with the Loewenstein rule of AlAl pair avoidance (Herrero and Sanz 1991). Then, this random distribution was included by imposing partial occupancies of Si and Al in the crystallographic positions of the tetrahedral sheet. In smectite/illite systems, spectroscopic studies and inverse MC simulations showed an MgMg pair avoidance and a partial short-range Fe segregation in the octahedral sheet, but no specific ordering was found (Cuadros et al. 1999). Besides, the cation ordering in the octahedral sheet is similar in the members of smectite/illite systems, and it does not significantly affect the crystal lattice parameters of these systems, since the experimental data are averaged values. Therefore, partial occupancies of Al, Mg, and Fe have been also included, taking into account the chemical composition of these cations. This approximation (called the virtual crystal approximation) can be considered valid as a common type of

Table 1 Interatomic potential parameters used in this work

Short-range interactions[a]	A (eV)	ρ (Å)	C (eV Å^{-6})	Reference[b]
Si^{4+}–O^{2-}	1283.9073	0.3205	10.6616	1
Si^{4+}–$O^{1.426-}$	999.98	0.3012	0.0	1
Al^{3+}–$O^{1.426-}$	1142.6775	0.2991	0.0	2
Al^{3+}–O^{2-}	1460.3	0.2991	0.0	1
(Fe^{3+}–O^{2-})[c]	3219.335	0.2641	0.0	3
Mg^{2+}–$O^{1.426-}$	1142.6775	0.2945	0.0	1
Mg^{2+}–O^{2-}	1428.5	0.2945	0.0	1
K^{+}–O^{2-}	65269.71	0.2130	0.0	1
Na^{+}–O^{2-}	1271.504	0.3000	0.0	3
Mg^{2+} (interlayer)–O^{2-}	946.627	0.31813	0.0	4
Ca^{2+}–O^{2-}	2272.74	0.2986	0.0	3
O^{2-}–O^{2-}	22764.0	0.149	27.88	1
$H^{0.426+}$–O^{2-}	325.0	0.25	0.0	1
Short-range interactions[d]	ε (eV)	α (Å^{-1})	μ (Å)	
$H^{0.426+}$–$O^{1.426-}$	7.0525	2.1986	0.9485	1
Shell-core interaction	K (eV Å^{-2})			
$O^{0.86902-}_{core}$–$O^{2.86902-}_{shell}$	74.92			1
Three-body bond bending	K (eV rad^{-2})	θ_o (°)		
O^{2-}–Si^{4+}–O^{2-}	2.09724	109.47		1
(O^{2-}–Al^{3+}(T)–O^{2-})[e]	2.09724	109.47		1
(O^{2-}–M(Oc)–O^{2-})[e]	2.09724	90		1
(O^{2-}–M(Oc)–$O^{1.426-}$)[e]	2.09724	90		
($O^{1.426-}$–M(Oc)–$O^{1.426-}$)[e]	2.09724	90		

[a] Parameters for the Buckingham potentials between cation cores and oxygen shells. When the parameter $C = 0.0$, the function takes the form of Born-Mayer potentials. Cutoff at 12 Å
[b] References: 1: Winkler et al. (1991); 2: Schröder et al. (1992); 3: Bush et al. 1994; 4: Gale (1997)
[c] With O^{2-}_{shell} or $O^{1.426-}_{core}$
[d] Modified Morse potential between cores
[e] T in the tetrahedral sheet; O_c in the octahedral coordination; M any cation in the octahedral sheet, Al^{3+}, Fe^{3+}, and Mg^{2+}

distribution for all samples, and as reference for our comparative studies.

The effects of nonstoichiometric chemical composition are simulated by using partial occupancies of various cations. This approach treats each distinct cation site as equivalent in each unit cell, and is a type of mean-field approach which is often called the virtual crystal approximation. Of course, it might be more realistic to use large supercells with a large number of disordered configurations. However, as well as having the penalty of making all calculations very demanding, the need for this approach is justified only when calculating very small changes in lattice parameters from ideal behavior (Bosenick et al. 2000b). In many cases (such as here), we do not require this level of accuracy, and the virtual crystal approximation has been used to great effect in a number of studies of the behavior of disordered crystals from a structural perspective (Winkler et al. 1991; Dove et al. 1993; Dove and Redfern 1997). The main problem with the virtual crystal approximation is in calculations of energies, and in the present case we are not concerned with energies. We use a supercell approach in applications of the present models for which energies are important (Palin et al. 2000).

The initial geometry of muscovite was taken from experimental structural data (powder neutron diffraction) of 2*M*1 muscovite (Catti et al. 1994). The experimental crystal structure of margarite was taken from Kassner et al. (1993). The pyrophyllite experimental structural data were taken from X-ray diffraction studies (Wardle and Brindley 1972). In the smectite/illite samples, no experimental atomic coordinates was available. Nevertheless, the initial geometries were taken from the models proposed by Tsipursky and Drits (1984) by means of oblique-texture electron diffraction studies of dioctahedral smectites. The experimental hydrogen positions of pyrophyllite, smectites, and illites were taken from the Giese (1979) studies on pyrophyllite, and these positions were optimized previously by us.

Results

Muscovite

Initially, the well-known crystal structure of muscovite was studied in order to validate the potential set used in this work. Two compositions were calculated (Table 2): one with Fe and Mg substitution in the octahedral sheet [$K_{0.95}(Al_{1.65}Fe^{3+}_{0.2}Mg_{0.15})(Si_{3.2}Al_{0.8})O_{10}(OH)_2$, musco1], and one end-member muscovite [$KAl_2(Si_3Al_1)O_{10}(OH)_2$, musco2]. Although the structural parameters of individual muscovite crystals can be measured accurately, the variation of parameters between different crystals can be significant because of differences in chemical composition. The structural features calculated were compared with experimental data of samples that have composition similar to the samples studied: a muscovite from a granite pegmatite dike [$K_{0.9}Na_{0.07}$)($Al_{1.63}Fe^{3+}_{0.23}Mg_{0.16}Ti_{0.03}$)($Si_{3.2}Al_{0.8}$)$O_{10}(OH)_2$, Catti et al. 1994] and a muscovite from Panasqueira (Portugal) [$K_1Na_{0.03}Ca_{0.01}$)($Al_{1.93}Fe^{3+}_{0.01}Mg_{0.01}Mn^{3+}_{0.01}$) ($Si_{3.09}Al_{0.91}$)$O_{10}(OH)_{1.88}F_{0.12}$, Guggenheim et al. 1987] for the musco1 and musco2 samples, respectively. In both cases, a good agreement with the experimental structural data was found. The values calculated for musco2 are consistent with the previous Collins and Catlow (1992) studies in an end-member muscovite. The main

Table 2 Comparison of simulated and experimental structural features of muscovite (lengths in Å and angles in degrees)

Parameters	Musco1[a]		Musco2[b]			Marga[c]	
	Exp.	Calc.	Exp.	Calc.	Calc.[d]	Exp.	Calc.
a	5.21	5.16	5.16	5.17	5.25	5.11	5.11
b	9.04	9.03	8.95	9.02	9.18	8.86	8.86
c	20.02	19.8	20.07	19.75	19.78	19.18	18.64
β	95.8	96.1	95.7	96.1	96.5	95.5	95.3
Tetrahedral sheet							
Mean T–O	1.643	1.659	1.636	1.647	1.620	1.683	1.691
τ[e]		112.0	109.5	110.4	107.5	110.4	111.0
ΔZ[f]	0.23	0.20	0.21	0.23	0.33		
Thickness	2.25	2.21	2.23	2.21	2.23		
Octahedral sheet							
Mean M–O	1.94	1.89	1.92	1.90	1.93	1.90	1.88
O–H	0.947	0.963		0.979	0.975	0.941	0.983
$\psi_{oct.}$[g]	57.3	58.9	57.1	57.1	56.9		
Thickness	1.73	2.08	2.08	2.06	2.11		
Interlayer separation	3.45	3.26	3.43	3.22	3.25		

[a] Experimental data of $(K_{0.9}Na_{0.07})(Al_{1.63}\ Fe^{3+}_{0.23}Mg_{0.16}Ti_{0.03})(Si_{3.2}Al_{0.8})O_{10}(OH)_2$ muscovite (Catti et al. 1994), and theoretical results of $K_{0.95}(Al_{1.65}Fe^{3+}_{0.2}Mg_{0.15})(Si_{3.2}Al_{0.8})O_{10}(OH)_2$

[b] Experimental data of Panasqueira muscovite $(K_1Na_{0.03}Ca_{0.01})(Al_{1.93}Fe^{3+}_{0.01}Mg_{0.01}Mn^{3+}_{0.01})(Si_{3.09}Al_{0.91})O_{10}(OH)_{1.88}F_{0.12}$ (Guggenheim et al. 1987), and theoretical results for $KAl_2\ (Si_3Al_1)O_{10}(OH)_2$

[c] Experimental data of margarita from Greiner (Tyrol, Austria), $(Ca_{0.73}Na_{0.21})\ (Al_{2.01}Fe^{3+}_{0.03}Mg_{0.1}Li_{0.12})\ (Si_{1.94}Al_{2.06})O_{10}(OH)_2$ (Kassner et al. 1993), and theoretical results for $Ca_1Al_2(Si_2Al_2)O_{10}(OH)_2$

[d] Calculated by Collins and Catlow (1992) for $KAl_2(Si_3Al_1)O_{10}(OH)_2$

[e] The O_{basal}–T–O_{apical} bond angle, τ

[f] Corrugation effect of basal surfaces

[g] Octahedral flattening angle, ψ, cos ψ = [oct. thickness/2(M–O)]

structural parameters (*a*, *b*, *c*, and β) are well reproduced by means of our calculations in both samples. In the tetrahedral sheet, the corrugation effect of the basal surface (departure from coplanarity of the basal oxygens, ΔZ) observed experimentally is reproduced in our calculations. The mean T–O bond length is also modeled well. The O_{basal}–T–O_{apical} bond angles, τ, are calculated to be slightly greater than the ideal undisturbed value of 109.47°. However, the calculated values match quite well with the average value of different experimental values (110.6–111.0°, Bailey 1980). In the octahedral sheet, the M–O bond length calculated is slightly shorter than the experimental value, probably due to the compositional differences. In all cases the O–H bond length calculated is slightly longer than the experimental one, since the repulsion between this hydrogen and the potassium cation is not well determined.

Margarite

An end member of brittle mica with a very strong interlayer charge [margarite, $Ca_1Al_2(Si_2Al_2)O_{10}(OH)_2$] was also modeled reproducing the experimental data [for $(Ca_{0.73}Na_{0.21})(Al_{2.01}Fe^{3+}_{0.03}Mg_{0.1}Li_{0.12})(Si_{1.94}Al_{2.06})O_{10}(OH)_2$, Kassner et al. 1993] from Greiner, Tyrol, Austria) of the main structural features (Table 2). The cell parameters calculated match quite well with the experimental values except *c*. This parameter *c* is slightly lower than the experimental value, probably due to compositional differences. Both values, theoretical and experimental, are lower than in the muscovite crystals due to the higher interlayer charge in margarite. The strong electrostatic field, produced by the high interlayer charge, reduces the interlayer d(001) distance. The theoretical cation-oxygen bond lengths (T–O and M–O in tetrahedral and octahedral sheets, respectively) reproduce the experimental values. The T–O bond length is longer than in the muscovite crystal due to the higher Al content in the tetrahedral sheet. As in previous samples, the theoretical O–H bond length is longer than the experimental one.

Pyrophyllite

After validating our potential model for phyllosilicates with high interlayer charge, like muscovite and margarite, this potential set was also applied to the study of 2:1 phyllosilicates with the minimal interlayer charge, like pyrophyllite $[Si_4Al_2O_{10}(OH)_2]$. Our calculations reproduce the main structural features of pyrophyllite with a good agreement with experimental values $[(Si_{3.98}Al_{0.02})(Al_{1.97}\ Fe^{3+}_{0.03})O_{10}(OH)_2$, Lee and Guggenheim 1981] (Table 3). The average disagreement level is lower than 2% in distances and angles, except in the parameter *c*. The theoretical value of the *c* parameter is lower than the experimental one, due to the nonexistence of interlayer charge. Without interlayer charge, there is no cation in the interlayer space and the existing interactions are too weak to be simulated accurately by our potential set. In the tetrahedral sheet, the Si–O and O–O bond

Table 3 Comparison of simulated and experimental structural features of pyrophyllite (lengths in Å and angles in degrees)

Parameters	Calc.[a]	Exp. 1[b]	Exp. 2[c]
a	5.14	5.16	5.16
b	9.06	8.96	8.97
c	8.14	9.35	9.35
α	91.6	91.0	91.2
β	101.8	100.4	100.5
γ	89.7	89.7	89.6
Tetrahedral sheet[d]			
Mean T–O	1.62	1.62	1.62
Mean O–O	2.648	2.640	2.640
Mean O–T–O	109.4	109.5	109.4
Mean Si–O–Si	134.2		136.0
τ[e]	108.0		109.2
α[f]	8.0		10.2
ΔZ[g]	0.2		0.24
Thickness	2.14		2.15
Octahedral sheet[h]			
Mean M–OH	1.91		1.89
Mean M–O	1.90	1.94	1.91
Mean O–H	0.986		
Mean OH–OH	2.334		2.338
Mean O–O	2.827	2.835	2.813
Mean HO–M–OH	75.2		76.5
Thickness	2.04		2.08
ψ^{i}_{oct}	55.2		57.0

[a] Calculated for $Si_4Al_2O_{10}(OH)_2$
[b] Experimental data from Wardle and Brindley (1972)
[c] Experimental data of $(Si_{3.98}Al_{0.02})(Al_{1.97}\ Fe^{3+}_{0.03})O_{10}(OH)_2$ (Lee and Guggenheim 1981)
[d] T is the cation of the tetrahedral sheet
[e] The O_{basal}–T–O_{apical} bond angle, τ
[f] Tetrahedral rotational angle, $\alpha = 1/2\ |120° - \text{mean}\ (O_bO_bO_b)|$
[g] Corrugation effect of basal surfaces
[h] M is the cation of the octahedral sheet
[i] Octahedral flattening angle, ψ, $\cos\psi$ = [oct. thickness/2(M–O)]

lengths and the O–Si–O bond angle match quite well with the experimental values. Similar agreement was found in the M–OH, M–O, OH–OH, O–O distances of the octahedral sheet. The rotation (α) and thickening (τ) angle of the tetrahedra are slightly underestimated in the calculations. The thickness of the tetrahedral and octahedral sheets and the corrugation effect are well reproduced. Hence, only the interlayer spacing is not well reproduced by this method. Studies at a higher level of theory, like quantum-mechanical calculations, are being performed in order to obtain better agreement with experimental data.

Group of beidellite, montmorillonite, and other smectites and illites

In order to assess the potential transferability of this model to most members of the 2:1 dioctahedral phyllosilicates, we have extended this study to a series of smectite/illites that are defined in Table 4. A wide range of tetrahedral, octahedral, and interlayer charges is considered (Table 4) by introducing different cation substitutions of Si^{4+} by Al^{3+} in the tetrahedral sheet, and Al^{3+} by Mg^{2+} and Fe^{3+} in the octahedra. In this series, there are samples without tetrahedral charge, like sme1 (end member of montmorillonite), sme2 (with more Mg^{2+} content and then higher octahedral charge than sme1), and sme3 (with the present of Fe^{3+}). Samples with a high tetrahedral charge, like sme19 (as a mica), have been also included. There are also members without octahedral charge like the end members of beidellite (sme5 and sme13), and samples with high octahedral charge (sme6). Samples with a very high Fe content (25 and 45%, in sme17 and sme18, respectively) in the octahedral sheet have also been included. There are also samples with a very low interlayer charge (sme4) and with a high interlayer charge (sme6 and sme19). Additionally, different interlayer cations have been also used (K^+, Na^+, Mg^{2+}, and Ca^{2+}).

Table 4 Chemical composition of the smectite/illite samples studied. Structural formulas on the basis $O_{20}(OH)_4$

Sample	Si^{4+}	Al^{3+} (T)	Al^{3+} (Oc)	Mg^{2+}	Fe^{3+}	Interlayer cation
sme1	8		3.5	0.5		$Na_{0.5}$
sme2	8		3	1		Na_1
sme3	8		2.8	0.7	0.5	$K_{0.7}$
sme4	7.9	0.1	3.9	0.1		$K_{0.2}$
sme5	7.6	0.4	4			$Na_{0.4}$
sme6	7.6	0.4	2.4	1.6		K_2
sme7	7.2	0.8	3.3	0.7		$Na_{1.5}$
sme8	7.2	0.8	3.3	0.7		$Mg_{0.75}$
sme9	7.2	0.8	3.3	0.7		$Ca_{0.75}$
sme10	7.2	0.8	3.3	0.7		$K_{1.5}$
sme11	7.2	0.8	3.5	0.5		$K_{1.3}$
sme12	7.2	0.8	3.7	0.3		$K_{1.1}$
sme13	7.2	0.8	4			$K_{0.8}$
sme14	7.2	0.8	3	0.5	0.5	$Na_{1.3}$
sme15	7.2	0.8	3	0.5	0.5	$K_{1.3}$
sme16	7.13	0.87	3.3	0.7		$K_{1.57}$
sme17	7.13	0.87	2	1	1	$K_{1.87}$
sme18	7	1	1.8	0.4	1.8	$K_{1.4}$
sme19	6.5	1.5	3.5	0.5		K_2

Some preliminary considerations should be presented in the modeling of the interlayer space interactions with the exchange cations. The K–O potential, taken from modified electron gas calculations (Post and Burnham 1986), describes quite well the interlayer interactions for a wide range of K content and interlayer charges. However, the Ca–O potentials taken from the same source (A = 6958.3, $\rho = 0.2516$) did not yield a good geometry (low value for the parameter c, 9.27) in the simulation of Ca smectites. Applying the Ca–O potentials (Table 1) from Bush et al. (1994), which gave good results for garnets (Bosenick et al. 2000a), the experimental data were reproduced in our calculations. Bush et al. extended the shell model to the Ca cation (q_{core}/q_{shell}: 0.719/1.281, K_s = 34.05). We applied this extension in our samples, but no improvement was obtained. Similarly the Na–O potential (A = 5836.824 eV, $\rho = 0.2411$), taken from Post and Burnham (1986), did not correctly describe the crystal structure (low values of c, 9.26). By using the Na–O potentials of Bush et al.

(1994), a good crystal structure was obtained with a high value of β. When the Mg^{2+} is as an interlayer cation, the interactions with the basal oxygens are different from that in the octahedral sheet. At first, we applied the same potentials for both kinds of Mg cations, but the geometry obtained had too low a parameter c (c = 9.07 Å). Applying the Mg–O potential from Lewis and Catlow (1985) for the interlayer Mg cations (A = 821.6, ρ = 0.3242), geometry with low c parameter (c = 9.29 Å) was also obtained. However, a better geometry was obtained by using the Mg–O potential from Gale (1997) (Table 1). These empirical potentials have been taken from crystals with strong interatomic interactions, and it is difficult to transfer them accurately to environments with softer interactions as in the interlayer space of clays. The interaction between the interlayer cation and the basal oxygens is much weaker than when both (cation and oxygen) are inside the crystal lattice. Thus, the parameter A in the Buckingham function can be generally lower for the interlayer cation than for the octahedral cation.

In most of smectite/illite samples, the calculated structural features (Table 5) are consistent with the experimental values (Tsipursky and Drits 1984). No important difference in the crystal cell parameters is observed with the cation substitution in the tetrahedral and octahedral sheet. In the samples with Ca^{2+} or Mg^{2+} as interlayer cations, the values of parameters c and β are slightly lower than in the rest of the series. Probably the repulsion term of these M^{2+}–O potentials is underestimated. In samples with extremely low interlayer charge (sme4), the crystal structure is consistent with the rest of the series, except the parameter c, that is slightly higher, probably due to the weakness of the interactions in the interlayer space. These results are consistent with previous calculations performed on pyrophyllite and beidellite (Teppen et al. 1997).

Discussion

In the smectites and illites, the resolution of the experimental diffraction data is too low to give information about the crystal structure, due to structural disorder and the small size of the crystals in clay minerals. The good agreement level between experimental and theoretical values obtained above shows us that we can predict theoretically some structural features for the crystal lattice of these smectite/illite series. Thus, we have calculated some features of the crystal lattice that are difficult to obtain experimentally, such as the thickness of the tetrahedral sheet, and octahedral sheet, corrugation effect of the basal oxygens of the tetrahedral (ΔZ), thickening of tetrahedra (τ), flattening of octahedra (ψ), and the O–H, T–O, M–O bond lengths (Table 5). In this series, the interlayer and octahedral sheet thicknesses are slightly higher than in muscovite, due to lower charge excess. On the contrary, the tetrahedral sheet thickness and the T–O bond length are slightly lower than in micas, due to the lower Al content in the tetrahedral sheet.

Cation substitution effect on the main crystal lattice parameters

The wide range of different cation substitution used in this work allows us to study the effect of the cation substitution on the crystal structure. From experimental results, some previous statistical studies on layer silicates were performed for correlating the parameter b with the cation composition. However, no general equation for all dioctahedral layers 2:1 silicates has been obtained yet, due to the wide variety of the natural samples (Brown and Brindley 1980). No example of this correlation has been reported in smectites. From our calculations in these smectite/illite systems, some partial relationships can be studied for the cation substitution effect on the parameter b. The increase in Fe^{3+} content produces a slight decrease of b, obtaining a good linear correlation (R = 0.9954). On the other hand, an increase of the interlayer charge produces an increase in b with a linear correlation (R = 0.9882). However, these last partial comparisons have been obtained taking into account a small number of series members. Nevertheless, a multiple correlation between the calculated values of b (in Å) and cation substitution can be obtained for all our samples yielding the equation:

$$b = 8.883(6) + 0.025(6)\,Al^{IV} + 0.016(6)\,Mg - 0.112(8)\,Fe^{3+} \quad (R^2 = 0.9324)\ , \tag{4}$$

where the numbers in parentheses are the standard deviations in the last decimals, and Al^{IV}, Mg, Fe^{3+} represent the cation composition for unit cell $[O_{20}(OH)_4]$.

A decrease in the calculated parameter c is observed with the increase in the Mg content presenting a linear correlation. Thus, in our calculations on potassium smectite/illite samples with a unit cell composition $K_{(0.8+x)}(Si_{7.2}Al_{0.8})(Al_{4-x}Mg_x)O_{20}(OH)_4$, the Mg substitution effect on c (in Å) can be expressed quantitatively by the equation:

$$c = 10.25 - 0.21\,Mg \quad (R = 0.9898)\ . \tag{5}$$

For a wider range of samples $M_{(y+x)}(Si_{7-y}Al_y)(Al_{4-x}Mg_x)O_{20}(OH)_4$ (M = K or Na, y = 0–0.87, and x = 0–1.6), in our calculations a similar correlation can be found (Fig. 1) yielding the equation:

$$c = 10.24 - 0.18\,Mg \quad (R = 0.9592)\ . \tag{6}$$

The increase in Mg content in the octahedral sheet produces an increase in the interlayer charge and attractive interactions in the interlayer space decreasing the interlayer d(001) spacing. Taking into account the experimental values published by Tsipursky and Drits (1984), the parameter c was correlated with the Mg

Table 5 Structural features of the smectite/illite samples (distances in Å and angles in degrees)[a]

Sample	*a*	*b*	*c*	*β*	T th.[b]	O. th.[b]	I. th.[b]	ΔZ	τ	ψ_{oct}^{c}	d(O–H)	T–O	M–O	M–OH
sme1[d]	5.22 (5.18)	8.89 (8.97)	10.20 (10.05)	101.3 (100.4)	2.11	2.09	3.56	0.17	111.5	56.63	0.979	1.615	1.903	1.924
sme2[d]	5.23 (5.18)	8.9 (8.97)	10.22 (10.05)	105.7 (100.4)	2.17	2.17	3.38	0.17	111.7	55.65	0.977	1.617	1.920	1.933
sme3[e]	5.23 (5.18)	8.84 (8.97)	10.26 (10.20)	103.3 (101.3)	2.11	2.14	3.51	0.19	111.2	55.63	0.980	1.615	1.895	1.855
sme4[d]	5.2 (5.18)	8.9 (8.97)	10.6 (10.05)	102.2 (100.4)	2.09	2.06	4.05	0.17	109.9	56.95	0.981	1.615	1.892	1.916
sme5	5.21	8.89	10.12	100.8	2.09	2.06	3.51	0.18	109.9	56.97	0.981	1.620	1.890	1.915
sme6[f]	5.2 (5.18)	8.92 (8.98)	9.96 (10.05)	102.0 (101.4)	2.21	2.16	3.14	0.12	113.3	56.32	0.982	1.625	1.945	1.957
sme7[f]	5.23 (5.18)	8.92 (8.98)	10.12 (10.05)	105.0 (101.4)	2.17	2.15	3.25	0.19	111.7	55.80	0.979	1.629	1.913	1.932
sme8[g]	5.24 (5.18)	8.89 (8.97)	9.48 (10.10)	96.7 (100.5)	2.11	2.09	2.82	0.17	111.5	56.88	0.979	1.629	1.914	1.929
sme9[h]	5.23 (5.18)	8.91 (8.98)	9.75	98.4 (99.6)	2.12	2.10	3.06	0.18	111.6	56.70	0.979	1.629	1.913	1.930
sme10[f]	5.22 (5.18)	8.92 (8.98)	10.09 (10.05)	102.6 (101.4)	2.15	2.13	3.30	0.18	111.8	56.19	0.979	1.628	1.914	1.933
sme11[f]	5.22 (5.18)	8.91 (8.98)	10.15 (10.05)	102.5 (101.4)	2.14	2.12	3.34	0.19	111.3	56.23	0.979	1.628	1.907	1.929
sme12[f]	5.2 (5.18)	8.9 (8.98)	10.19 (10.05)	102.4 (101.4)	2.12	2.10	3.45	0.19	110.9	56.46	0.979	1.628	1.900	1.925
sme13	5.21	8.90	10.24	102.3	2.11	2.08	3.55	0.20	110.2	56.63	0.981	1.628	1.891	1.918
sme14[i]	5.22 (5.20)	8.85 (9.01)	10.04 (10.20)	100.4 (101.3)	2.10	2.12	3.30	0.20	111.3	55.98	0.982	1.628	1.891	1.854
sme15[i]	5.23 (5.20)	8.86 (9.01)	10.16 (10.20)	102.3 (101.3)	2.12	2.13	3.38	0.21	111.4	55.76	0.982	1.627	1.892	1.856
sme16[f]	5.22 (5.18)	8.93 (8.98)	10.08 (10.05)	102.5 (101.4)	2.16	2.13	3.28	0.18	111.8	56.25	0.977	1.630	1.914	1.933
sme17[i]	5.22 (5.20)	8.81 (9.01)	10.09 (10.20)	102.0 (101.3)	2.17	2.16	3.25	0.17	112.7	55.15	0.988	1.629	1.892	1.788
sme18[i]	5.23 (5.20)	8.57 (9.01)	10.29 (10.20)	101.4 (101.3)	2.16	2.16	3.49	0.25	111.4	53.88	0.999	1.630	1.832	1.599
sme19	5.22	8.94	10.03	102.3	2.17	2.12	3.20	0.19	111.3	55.98	0.980	1.639	1.891	1.854

[a] Values in brackets correspond to experimental data from Tsipursky and Drits (1984) of those I/S samples with the closest composition to our samples

[b] T th.: tetrahedral sheet thickness, O. th.: octahedral sheet thickness, I. th.: interlayer thickness

[c] Flattening angle of octahedral [cos ψ = O. th./2(M–O)]

[d] Experimental data from $(Ca_{0.06}K_{0.09}Na_{0.17})(Al_{1.38}Fe^{3+}_{0.14}Mg_{0.48})(Si_{3.98}Al_{0.02})O_{10}(OH)_2$

[e] Experimental data from $(Ca_{0.06}K_{0.07}Na_{0.17})(Al_{1.39}Fe^{3+}_{0.26}Fe^{2+}_{0.05}Mg_{0.3})Si_4O_{10}(OH)_2$

[f] Experimental data from $(Ca_{0.06}K_{0.27}Na_{0.21})(Al_{1.64}Fe^{3+}_{0.05}Mg_{0.31})(Si_{3.71}Al_{0.29})O_{10}(OH)_2$

[g] Experimental data from $(Ca_{0.1}K_{0.05}Na_{0.05}Mg_{0.27})(Al_{1.05}Fe^{3+}_{0.37}Mg_{0.57})(Si_{3.73}Al_{0.27})O_{10}(OH)_2$

[h] Experimental data from $(Ca_{0.22}K_{0.04}Na_{0.01})(Al_{1.38}Fe^{3+}_{0.18}Mg_{0.44})(Si_{3.95}Al_{0.05})O_{10}(OH)_2$

[i] Experimental data from $(Ca_{0.11}K_{0.16}Na_{0.03})(Al_{0.96}Fe^{3+}_{0.88}Mg_{0.26})(Si_{3.53}Al_{0.47})O_{10}(OH)_2$

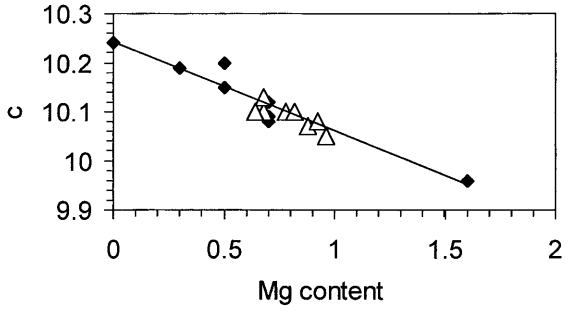

Fig. 1 Relationship between the Mg content [based on the structural formulas for $O_{20}(OH)_4$] in the octahedral sheet and the parameter c (in Å). Calculated (*solid symbols*) and experimental (*open symbols*) values

content obtaining a similar relationship to our theoretical results in Eq. (6) (Fig. 1) with the equation:

$$c = 10.22 - 0.17\,\mathrm{Mg} \quad (R = 0.8227) \ . \tag{7}$$

Cation substitution effect on the sheet thickness

The known effect of the interlayer charge on the interlayer thickness is well reproduced in our calculations. The interlayer thickness decreases with the increase in the interlayer charge. The cation substitution can produce a charge excess that is localized mainly in the basal oxygens of the tetrahedral sheet. The higher the charge, the stronger is the interaction between these oxygens and the interlayer cations. Hence, this increase in interaction strength produces a decrease in the interlayer thickness. Linear correlations can be found for both parameters (Fig. 2a), considering the octahedral charge effect (with the tetrahedral charge as a constant, $R = 0.9937$) and the tetrahedral charge effect (with the octahedral charge as a constant, $R = 0.9938$). For samples, $K_{(0.8+x)}(Al_{4-x}Mg_x)(Si_{7.2}Al_{0.8})O_{20}(OH)_4$, the octahedral charge effect on the interlayer thickness (in Å) can be expressed quantitatively by the equation:

$$\text{Interlayer thickness} = 3.55 - 0.37 q_{\mathrm{oct}} \ , \tag{8}$$

where q_{oct} is the octahedral charge per unit cell. In the same way, for samples $K_{(0.5+x)}(Si_{8-x}Al_x)\ (Al_{3.5}Mg_{0.5})O_{20}(OH)_4$, the tetrahedral charge effect on the interlayer thickness (in Å) can be expressed quantitatively by the equation:

$$\text{Interlayer thickness} = 3.50 - 0.21 q_{\mathrm{tetra}} \ , \tag{9}$$

where q_{tetra} is the tetrahedral charge per unit cell. The octahedral charge effect is similar to the tetrahedral charge effect, but with a slightly higher slope increasing the effect in the octahedral charge. When the charge excess comes from the octahedral sheet, the cations can more likely approach into the hexagonal hole of the tetrahedral layer, decreasing the interlayer distance. This phenomenon could explain the slightly higher sensitivity

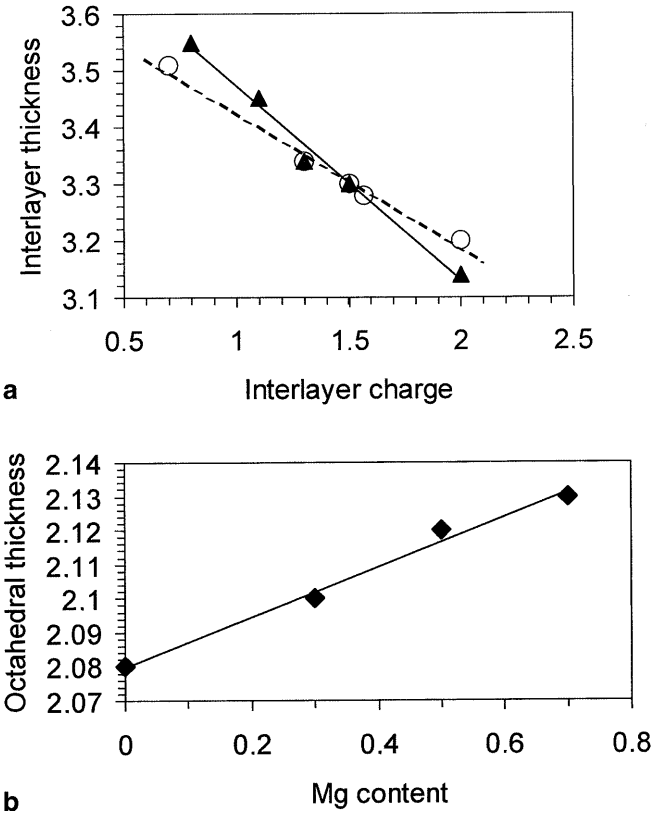

Fig. 2a, b Effects of cation substitution on interlayer and octahedral sheet thickness (in Å). Interlayer thickness vs. interlayer charge (**a**) (*solid* and *dotted lines* for series with tetrahedral composition constant and series with octahedral composition fixed, respectively), and (**b**) octahedral sheet thickness vs. Mg content based on the $O_{20}(OH)_4$ formula

of the interlayer thickness to the octahedral charge-increasing effect.

A slight increase in the octahedral sheet thickness with the increase in Mg content is observed, as expected, due to the higher ionic radius of Mg^{+2} (0.72 Å) with respect to Al^{+3} (0.54 Å). A linear relationship is found in this effect (Fig. 2b, $R = 0.9943$). Although there are only a few samples where all variables are constant except the Mg or Al^{IV} content, a semiquantitative estimation of the cation substitution can be performed. So, for samples $K_{(0.8+x)}(Al_{4-x}Mg_x)(Si_{7.2}Al_{0.8})O_{20}(OH)_4$, the Mg substitution effect on the octahedral sheet thickness (in Å) can be expressed by the equation:

$$\text{Octahedral thickness} = 2.08 + 0.07\,\mathrm{Mg} \ . \tag{10}$$

In the same way, a slight increase in tetrahedral sheet thickness is observed with an increase in tetrahedral Al content, probably due to a similar effect, the higher ionic radius of Al^{+3} with respect to Si^{+4}. In samples $K_{(0.5+x)}(Al_{3.5}Mg_{0.5})(Si_{8-x}Al_x)O_{20}(OH)_4$, the Al^{IV} substitution effect on the tetrahedral sheet thickness (in Å) can be expressed by the equation:

$$\text{Tetrahedral thickness} = 2.11 + 0.04\,\mathrm{Al^{IV}} \ . \tag{11}$$

Cation substitution effect on the distortion parameters

In 2:1 layer aluminosilicates, distortions from an ideal hexagonal tetrahedral or octahedral sheet can be produced. The larger tetrahedral sheet can reduce its lateral dimensions to compensate for the smaller size of the octahedral sheet. Alternatively, the octahedral sheet may expand its lateral dimensions to partly compensate for this misfit. One of the structural distortions is the corrugation effect (ΔZ) of basal tetrahedral oxygens along [110], producing a tilting of the tetrahedral out of the (001) plane. The ΔZ values found in these smectite/illite samples are similar to those found in mica and pyrophyllite. No specific correlation was found between this parameter and the cationic substitutions. The sme18 sample presented a slightly higher ΔZ, due to the distortions produced by the high substitution grade of Fe. Another distortion parameter is the thickening effect of the tetrahedra (τ, determined by the O_{basal}–T–O_{apical} bond angles). The values calculated are slightly larger than the ideal undisturbed value of 109.47°, as it was found in micas above. A linear correlation was found between this parameter and the Mg substitution in the octahedral sheet (Fig. 3a, $R = 0.9836$). An increase in τ with the increase in Mg content is found. The higher ionic radius of the Mg makes it push out the apical tetrahedral oxygens, increasing this O_{basal}–T–O_{apical} bond angle. In potassium samples with a composition in the range of 0.4–0.87 and 0–1 atoms per unit cell of Al^{IV} and Fe^{3+}, respectively, the Mg substitution effect on τ (in degrees) can be expressed quantitatively by the equation:

$$\tau = 110.34 + 2.01\,\mathrm{Mg} \quad . \tag{12}$$

The flattening effect of the octahedra is another distortion parameter in these structures (Ψ, determined by the angle between the normal to the octahedral sheet and a body diagonal of the octahedron, the ideal value is 54.7°). All smectite/illite samples present values of Ψ in the same range as is found in micas and pyrophyllite (Guven 1988). Some relationships between this parameter and the cation substitutions can be found. A decrease in Ψ with the increase in Fe content is found with a linear correlation (Fig. 3b, open symbols, $R = 0.9939$). For potassium samples with a composition of 0.8–1.0 and 0.4–1.0 atoms per unit cell of Al^{IV} and Mg, respectively, the Fe^{3+} substitution effect on Ψ (in degrees) can be expressed quantitatively by the equation:

$$\Psi = 56.35 + 1.33\,\mathrm{Fe}^{3+} \quad . \tag{13}$$

Analogously, the Ψ decreases slightly with the increasing of the interlayer charge, showing also a linear correlation (Fig. 3b, solid symbols, $R = 0.9857$). For potassium samples with a cation composition of 0.1–1.5 and 0–0.7 atoms per unit cell of Al^{IV} and Mg, respectively, the interlayer charge (IC) effect on Ψ (in degrees) can be expressed quantitatively by the equation:

$$\Psi = 57.05 - 0.55\,\mathrm{IC} \tag{14}$$

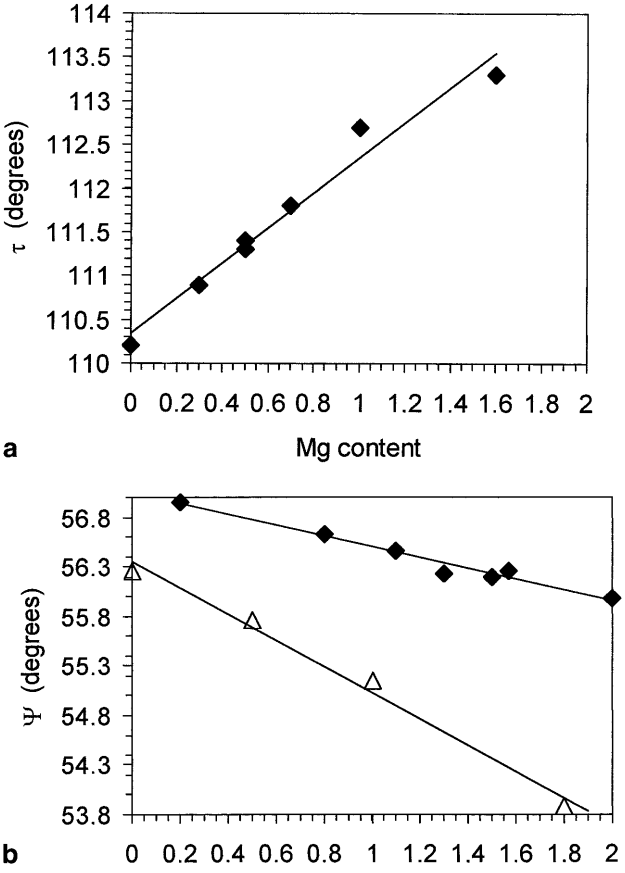

Fig. 3a, b Variation of the distortion parameters with cation substitutions. (**a**) Thickening effect of the tetrahedra (τ) vs. Mg content per $O_{20}(OH)_4$. (**b**) Flattening effect on the octahedra (ψ) vs. Fe content (*open symbols*) and interlayer charge (*solid symbols*) per $O_{20}(OH)_4$

Effects on the main bond lengths

The previous structural parameters studied above are closely related with the main bond lengths of the crystal, and these bond lengths can also be affected by the cation substitutions. An increase in the T(tetrahedral cation)–O bond length with the tetrahedral Al content is observed with a good linear correlation (Fig. 4a, $R = 0.9973$). This fact is due to the higher ionic radius of Al^{3+} with respect to Si^{4+}. For all samples, a quantitative relationship of the Al^{IV} substitution effect on the T–O bond length (in Å) can also be found with the equation:

$$\mathrm{d(T\text{–}O)} = 1.614 + 0.017\,\mathrm{Al}^{IV} \quad . \tag{15}$$

Analogously, an increase of M(octahedral cation)–O bond length with the Mg content is found, also with a good linear correlation (Fig. 4b, solid symbols, $R = 0.9991$), due also to the higher ionic radius of Mg^{2+} (0.72 Å) with respect to Al^{3+} (0.54 Å). This effect of the Mg substitution on the M–O bond length (in Å) can also be expressed quantitatively with the equation:

$$\mathrm{d(M\text{–}O)} = 1.890 + 0.034\,\mathrm{Mg} \tag{16}$$

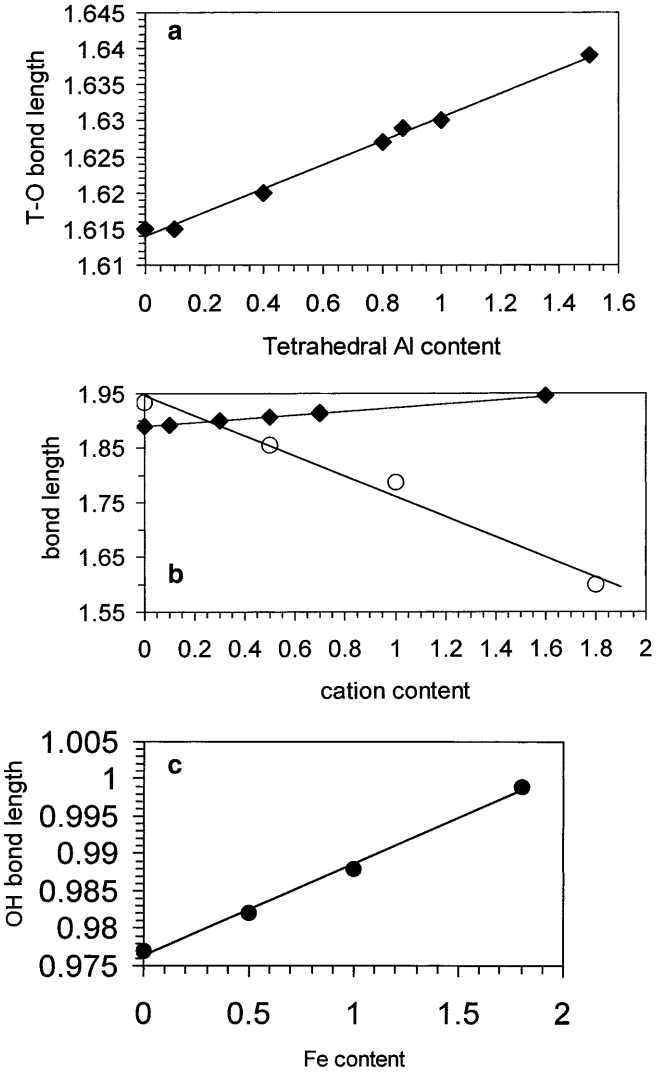

Fig. 4a–c Cation substitution effect on the T–O (**a**), Mg content on M–O (**b**, *solid symbols*), Fe content on M–OH (**b**, *open symbols*), and O–H (**c**) bond lengths (in Å) in smectite/illite samples

for all potassium smectite/illite samples that no have significant amount of Fe^{3+}. On the other hand, a decrease in the M–OH bond length with the increase in Fe content is observed, with also a good linear correlation (Fig. 4b, open symbols, $R = 0.9910$), in spite of the higher ionic radius of Fe^{3+} (0.65 Å) with respect to Al^{3+}. For potassium samples with a composition of 0.8–1.0 and 0.4–1.0 atoms per unit cell of Al^{IV} and Mg, respectively, a quantitative relationship of the Fe^{3+} substitution effect on the M–OH bond length (in Å) can be also found with the equation:

$$d(\text{M–OH}) = 1.946 - 0.184\,Fe^{3+} \quad . \tag{17}$$

This fact can be due to a higher covalent character of the Fe–O bond (a higher overlapping between the oxygen orbitals and the Fe d-orbitals) than the other M–O bonds in the octahedral sheet (Sherman 1985; Sainz-Diaz et al. 2000).

As found in previous simulation studies of hydroxyl ions in minerals, the experimental OH bond length is slightly shorter than the value calculated. Nevertheless, we observe a linear relationship between the OH bond length and the Fe content in the octahedral sheet (Fig. 4c, $R = 0.9975$). The OH bond length increases with the increase of Fe content. This relationship is independent of the octahedral and tetrahedral cation substitutions. A longer O–H bond length is related with a lower ν(OH) frequency. Hence, this is consistent with the experimental values of the stretching vibrational frequency ν(OH) of the M–OH–M groups, which decrease with the increase in Fe content (Besson and Drits 1997). This fact has been corroborated by means of quantum mechanical calculations on molecular clusters representing dioctahedral pairs of the octahedral sheet of clays (Sainz-Diaz et al. 2000).

Conclusions

The experimental crystal lattice structure of 2:1 dioctahedral phyllosilicates with high and low interlayer charge can be reproduced theoretically by means of a suitable simulation model. This model can be formed with a careful selection of transferable empirical potentials that have been used successfully in the modeling of framework silicates and other minerals. The selection of a suitable empirical potential set is critical for modeling 2:1 dioctahedral phyllosilicate crystal structures, due to the significant differences with other nonlayered silicates. The most peculiar characteristic of these phyllosilicates is the existence of the interlayer space, where the atomic interactions are much weaker than in the crystal lattice.

The muscovite, margarite, pyrophyllite, beidellite, montmorillonite, and other different smectites and illites can be modeled by means of this interatomic empirical potential set. The theoretical structural parameters of the mica muscovite (two different compositions), and the brittle mica margarite, both with high interlayer charge, match quite well the experimental values. A good agreement between calculated and experimental results has also been obtained in the pyrophyllite studies, where there is no interlayer charge, in any crystal lattice parameters except in c. The tetrahedral and octahedral sheet thicknesses are well described. Hence, our method did not properly describe the interlayer thickness in pyrophillite, due to the weakness of the interactions in this interlayer space. Extending the study to the rest of the series, beidellite, montmorillonite, and other smectites and illites, the transferability of our potential model has been assessed. These samples represent a wide range of interlayer charge (between mica and pyrophyllite types). In these silicates the agreement between experimental and theoretical results is similar to the results for micas and pyrophyllite.

In most cases, the interlayer space interactions have been reproduced satisfactorily, except in margarite and

pyrophyllite. In these last samples, the parameter c calculated is lower than the experimental value, due to composition differences (in margarite) or the existence of too weak interactions in the interlayer space (in pyrophyllite). Nevertheless, the calculated structures reproduce the experimental crystal lattice in the main structural features. The parameters calculated, which characterize the distortion of the tetrahedra and octahedra, are consistent with the experimental values. In all cases, the OH bond length calculated is slightly longer than the experimental values.

In smectite/illite samples, the cation substitution effect (in octahedral and tetrahedral sheets) on the structural features has been also studied. In most cases where the structural parameters are sensitive to these cation substitutions, good linear correlations have been found. Our theoretical results are consistent with the experiment in those cation substitution effects that have been detected experimentally, as in the (interlayer thickness)/(interlayer charge) relationship. In the same way, a linear relationship between the Fe content and the OH bond length has been found, in agreement with previous spectroscopic studies.

This good agreement between experimental and calculated values shows us that these theoretical simulations can be useful for predicting structural features of the crystal lattice of clays which cannot be obtained by experiment. Moreover the cation substitution effect on these predicted parameters can be studied by means of our calculations. The quality of the correlations obtained allows us to predict quantitative relationships between the cation substitution effects and the main structural features of the crystal lattice. Further calculations have to be performed for a wider range of cation substitutions, in order to increase the accuracy of these quantitative relationships and to generalize these cation substitution effects for all phyllosilicates. The predictive power of our calculations can be useful for understanding and refining low-resolution experimental X-ray or neutron diffraction studies of illites and smectites.

These results assess the validation of this potential selection set for application it in further studies on clays, such as order/disorder of cations by Monte Carlo simulations, mineral transformations, such as smectite/illite transition, diagenetic transformations in sediments, and *cis*-vacant/*trans*-vacant transformations.

Acknowledgements The authors are grateful to Dr. M. Warren for her useful support in the computing facilities, to Dr. J. Gale for his fruitful help and for permitting us to use the GULP program, and for the financial support of NERC (M. T. Dove), The Royal Society of UK and MEC of Spain (C.I. Sainz-Diaz), and the PB97-1205 DGES project (A. Hernández-Laguna) and Acciones Integradas UK/Spain joint research programme.

References

Abbot RN Jr, Post JE, Burnham CW (1989a) Treatment of the hydroxyl in structure-energy calculations. Am Mineral 74: 141–150

Abbot RN Jr, Burnham CW, Post JE (1989b) Hydrogen in humite-group minerals: structure-energy calculations. Am Mineral 74: 1300–1306

Bailey SW (1980) Structures of layer silicates. In: Brindley GW, Brown G (Eds) Crystal structures of clay minerals and their X-ray identification. Mineralogical Society, London, 1–123

Besson G, Drits VA (1997) Refined relationship between chemical composition of dioctahedral fine-grained micaceous minerals and their infrared spectra within the OH stretching region. Clays Clay Miner 45: 170–183

Bosenick A, Dove MT, Geiger CA (2000a) Simulation studies of pyrope-grossular solid solutions. Phys Chem Miner 27: 398–418

Bosenick A, Dove MT, Heine V, Geiger CA (2000b) Scaling of thermodynamic mixing properties in garnet solid solutions. Phys Chem Miner (submitted, awaiting revision)

Brown G, Brindley GW (1980) X-ray diffraction procedures for clay mineral identification. In: Brindley GW, Brown G (Eds) Crystal structures of clay minerals and their X-ray identification. Mineralogical Society, London, pp 305–360

Bush TS, Gale JD, Catlow CRA, Battle PD (1994) Self-consistent interatomic potentials for the simulation of binary and ternary oxides. J Mat Chem 4: 831–837

Catlow CRA (1988) Computer modeling of silicates. In: Salje EKH (Ed.) Physical properties and thermodynamics behaviour of minerals, NATO ASI Series C., Reidel, Boston, 225: 619–638

Catlow CRA, Mackrodt JR, Stewart RF (1982) Defect energies in aluminium oxide and rutile titanium oxide. Phys Rev B 25: 1006–1026

Catti M, Ferraris G, Hull S, Pavese A (1994) Powder neutron diffraction study of 2M1 muscovite at room pressure and at 2 Gpa. Eur J Miner 6: 171–178

Collins DR (1990) Computer simulation and neutron scattering studies of layer silicate minerals. PhD Thesis, University of Keele, UK

Collins DR, Catlow CR (1992) Computer simulations of structures and cohesive properties of micas. Am Mineral 77: 1172–1181

Cuadros J, Sainz-Diaz CI, Ramirez R, Hernández-Laguna A (1999) Analysis of Fe segregation in the octahedral sheet of bentonitic illite-smectite by means of FT-IR, ^{27}Al MAS NMR and reverse Monte Carlo simulations. Am J Sci 299: 289–308

Dove MT (1989) On the computer modeling of diopside: toward a transferable potential for silicate minerals. Am Mineral 74: 774–779

Dove MT, Redfern SAT (1997) Lattice simulation studies of the ferroelastic phase transitions in (Na,K)$AlSi_3O_8$ and (Sr,Ca)$Al_2Si_2O_8$ feldspar solid solutions. Am Mineral 82: 8–15

Dove MT, Cool T, Palmer DC, Putnis A, Salje EKH, Winkler B (1993) On the role of Al/Si ordering in the cubic–tetragonal phase transition in leucite. Am Mineral 78: 486–492

Gale JD (1997) GULP – a computer program for the symmetry adapted simulation of solids. J Chem Soc Faraday Trans 93: 629

Giese RF Jr. (1979) Hydroxyl orientations in 2:1 phillosilicates. Clays Clay Miner 27: 213–223

Guggenheim S, Chang Y-H, Koster van Groos AF (1987) Muscovite dehydroxylation: high-temperature studies. Am Mineral 72: 537–550

Guven N (1988) Smectites. In: Bailey SW (Ed) Hydrous phyllosilicates. Reviews in Mineralogy, vol. 19. Mineralogical Society of America 497–559

Herrero CP, Sanz J (1991) Short-range order of the Si,Al distribution in layer silicates. J Phys Chem Solids 52: 1129–1135

Jackson RA, Catlow CRA (1988) Computer simulation studies on zeolite structures. Mol Simul 1: 207–224

Kassner D, Baur WH, Joswig W, Eichhorn K, Wendschuh-Josties M, Kupcik V (1993) A test of the importance of weak reflections in resolving a space-group ambiguity involving the presence or absence of an inversion centre. Acta Crystallogr (B) Structural Science 49: 646–654

Lasaga AC, Gibbs GV (1987) Applications of quantum mechanical potential surfaces to mineral physics calculations. Phys Chem Miner 14: 107–117

Lee JH, Guggenheim S (1981) Single crystal X-ray refinement of pyrophyllite-1*Tc*. Am Mineral 66: 350–357

Lewis GV, Catlow CRA (1985) Potential models for ionic oxides. J Phys C 18: 1149–1161

Post JE, Burnham CW (1986) Ionic modeling of mineral structures and energies in the electron gas approximation: TiO_2 polymorphs, quartz, forsterite, diopside. Am Mineral 71: 142–150

Price GD, Parker SC (1988) The computer simulation of the lattice dynamics of silicates. In: Salje EKH (Ed) Physical properties and thermodynamics behaviour of minerals. NATO ASI Series C, Reidel, Boston, 225: 591–618

Sainz-Diaz CI, Timon V, Botella V, Hernández-Laguna A (2000) Isomorphous substitution effect on the vibration frequencies of hydroxyl groups in molecular cluster models of the clay octahedral sheet. Am Mineral 85: 1038–1045

Sauer J, Ugliengo P, Garrone E, Saunders VR (1994) Theoretical study of van der Waals complexes at surface sites in comparison with the experiment. Chem Rev 94: 2095–2160

Schröder K-P, Sauer J, Leslie M, Catlow CRA, Thomas JM (1992) Bridging hydroxyl groups in zeolitic catalysts: a computer simulation of their structure, vibrational properties and acidity in protonated faujasites (H-Y zeolites). Chem Phys Lett 188: 320–325

Sherman DM (1985) The electronic structures of Fe^{3+} co-ordination sites in iron oxides. Application to spectra, bonding and magnetism. Phys Chem Miner 12: 161–175

Teppen BJ, Rasmussen K, Bertsch PM, Miller DM, Schafer L (1997) Molecular dynamics modeling of clay minerals. 1. Gibbsite, kaolinite, pyrophyllite, and beidellite. J Phys Chem B 101: 1579–1587

Tsipursky SI, Drits VA (1984) The distribution of octahedral cations in the 2:1 layers of dioctahedral smectites studied by oblique-texture electron diffraction. Clay Miner 19: 177–193

Wardle R, Brindley GW (1972) The crystal structures of pyrophyllite-1Tc, and its dehydroxylate. Am Mineral 57: 732–750

Winkler B, Dove MT, Leslie M (1991) Static lattice energy minimization and lattice dynamics calculations on aluminosilicate minerals. Am Mineral 76: 313–331